Numerical Simulation of Drops Impacting on Textured Surfaces

Y.X. Wang, *S. Chen

School of Aerospace Engineering and Applied Mechanics, Tongji University, China.

*Corresponding author: schen_tju@tongji.edu.cn

Abstract

In the present study drops impacting on textured surfaces were investigated using many-body dissipative particle dynamics (MDPD). A novel linear-jointed solid/fluid interaction with short-range repulsive and long-range attractive forces was used to generate different wettability and a simple but efficient numerical method was introduced to measure the contact angle. A systematic study was carried out to obtain the relationship between initial impact velocity and spreading properties on surfaces with different wettability induced by chemistry and topology. The simulated results showed that the drop is easily rebounded at lower $\emptyset_S$ with high impact velocity and only spreading occurs at low impact velocity or larger $\emptyset_S$. Referring to the triple-phase contact line, the time-based retraction phase was divided into two periods, and it was analyzed from an energy transition and dissipation viewpoint. It is expected to provide simulation details for the water-repellency surfaces design.

Keywords: Drop, Impact, Contact angle, Surface roughness, Many-body dissipative particle dynamics

Introduction

For years, surface wetability, especially the superhydrophobicity, has been the focus of surface science. Superhydrophobicity can cause drop to roll very easily off solid surfaces or bounce back upon impacting, just like the lotus leaf which can make rain drops roll off in ball easily (Lotus effect) [Barthlott and Neinhuis (1997)]. Generally speaking, superhydrophobicity means that the contact angle is larger than 150 °while the contact angle hysteresis less than 10 °, which confers to drops a high mobility on these surfaces. Unfortunately, for smooth and flat surfaces the possible highest contact angle is less than 120 °if without special processing. In nature, there are many plants and animals showing superhydrophobicity besides the lotus leaf, such as the antifogging mosquito eyes [Gao et al. (2007)] and legs of a water strider [Gao and Jiang (2004)] and feathers of many birds. Recently, scientists decoded the mechanism of them and found that the microtextured and nanotextured roughness contributes significantly to the quality of the water-repellency property. This breakthrough has attracted lots of researches to investigate drop wetting states, such as the Cassie [Cassie and Baxter (1944)] and Wenzel [Wenzel (1936)] state (Figure 1 Left and Right), and dynamic behavior on textured surfaces. The Cassie state is often described as "air trapping" or composite surface which means the liquid bridges between surface protrusions and no longer penetrates the interspace where it is filled with air (Figure 1). Cassie and Baxter considered the contact angle on heterogeneous surfaces composed of two different materials (solid surface and air), in which $\emptyset_S$ and $1-\emptyset_S$ ($\emptyset_S = W/L$, Figure 1) are the fractional areas of the wetted solid/liquid and liquid/air interfaces, respectively. Based on this viewpoint, they gave the Cassie-Baxter theoretical formula, $\cos\theta_C = \emptyset_S \cos\theta_Y + (1-\emptyset_S)\cos 180°$. This formula shows that the trapped air always drives the Cassie angle, θ_C, from Young angle to a larger contact angle (Figure 2). Many researches show great interests on this kind of drop state. Singh et al. [Singhet al. (2013)] draped the nanotextured surface with a single-layer graphene sheet to avoid the water intruding into the textured surface features and keep the drop in an ideal Cassie state. Their experiment showed that the seperated drop on the graphene sheet could hardly be pinned to the substrate and the contact angle hysteresis was reduced significantly. Also, Kim et al. [Kim et al. (2012)] did a systematic research about drop impact characteristics on multiscaled rough surfaces and found only on the nanoscaled surface the drop could rebound completely. From the static and dynamic contact angle measurement results they found the nanostructures showed superhydrophobic properties and were close to the nonwetted state (Cassie state). The theoretical analysis and physical experiments show that the Cassie state can provide a smaller angle hysteresis as well as a larger contact angle, thence, in many industrial applications such as self-cleaning surfaces people show more interests in the Cassie state than the Wenzel state. However, in experiments it’s not easy to hold Cassie state when there exists higher impacting velocity of drop, which can cause a Cassie-to-Wenzel transition. However the ideal Cassie state without transition could be investigated by numerical method. In this paper, the drop spreading dynamics under different wettability and impact velocities in ideal Cassie state was studied by using a particle-based numerical method (MDPD).

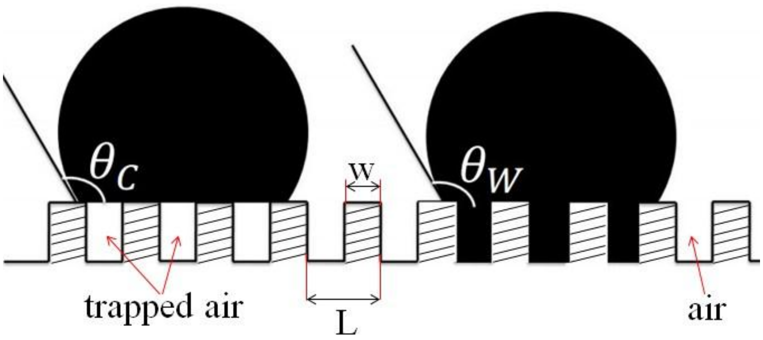

Figure 1 Drop states on textured surface

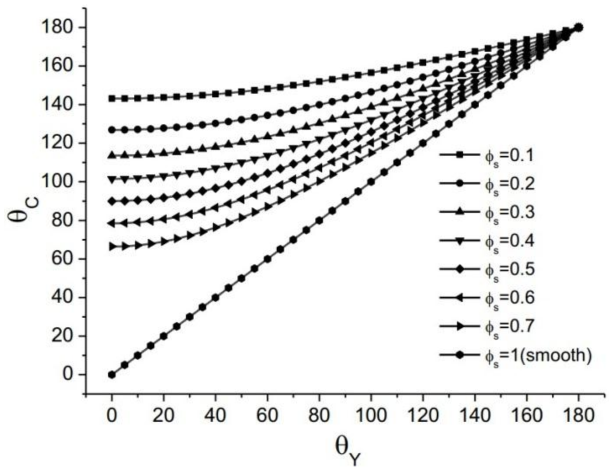

Figure 2 Theoretical Cassie angles on different rough surfaces

Computational method

MDPD

MDPD [Warren (2003); Trofimov et al. (2005)] is a modified numerical method of DPD [Hoogerbrugge and Koelman (1992); Groot and Warren (1997)] which includes the van der Waals loop in the EOS so as to make the DPD suitable for simulations of fluid systems with free surfaces. In the present work, we employ the MDPD scheme reported by Warren and in this scheme both the random and dissipative forces are kept the same with classical DPD while conservative force is revised as EQ.(1):

$$\mathbf{F}_{ij}^{C} = A\omega_c(r_{ij})\mathbf{e}_{ij} + B(\bar{\rho}_i + \bar{\rho}_j)\omega_d(r_{ij})\mathbf{e}_{ij} \tag{1}$$

in which $A\omega_c(r_{ij})\mathbf{e}_{ij}$ is the attractive part by setting A<0 and the weight function $\omega_c(r_{ij})$ is defined as the classical DPD, $\omega_c(r_{ij}) = 1 - r_{ij}/r_c$. $B(\bar{\rho}_i + \bar{\rho}_j)\omega_d(r_{ij})\mathbf{e}_{ij}$ is the repulsive part which depends on a weighted average of the local density by defining $\rho_i(r_{ij})$ as follows:

$$\rho_i(r_{ij}) = \sum_{i\neq j} \omega_\rho(r_{ij}) \tag{2}$$

$$\omega_\rho(r_{ij}) = 15/(2\pi {r_d}^3)(1 - r_{ij}/r_d)^2 \tag{3}$$

The weight functions ω_d in EQ.(1) are in similar definitions with $\omega_c(r_{ij})$, $\omega_d(r_{ij}) = 1 - r_{ij}/r_d$, but with different cutoff distances: $r_c = 1$ and $r_d = 0.75$.

Boundary Condition

To generate various hydrophobic and hydrophilic wetting behaviors, the solid/fluid conservative force is modeled by combining short-range repulsive and long-range attractive forces. Here, three linear weight functions are simply joined together and this is some different from the bell-shaped weight function of smoothed particle hydrodynamics.

$$F_{sl}^{C} = \begin{cases} F_b(1 - r_{ij}/r_d) & , \quad r_{ij} \leq r_b \\ F_a/(r_b - r_a)(r_b - r_{ij}) & , \quad r_b < r_{ij} \leq r_a \\ F_a/(r_{sl} - r_a)(r_{sl} - r_{ij}) & , \quad r_a < r_{ij} \leq r_{sl} \end{cases} \tag{4}$$

F_{sl}^{C} is the conservative force between solid and fluid particles which depends on their distance r_{ij} .The parameters F_a and F_b in EQ.(4) determine the strength of the attractive and repulsive interactions, r_{sl} is the wall-fluid interaction range and the two sub-ranges r_a and r_b are the positions of the maximum attractive force and the vanishing of the repulsive force (Figure 3). To simplify the simulation, F_b, r_{sl}, r_a and r_b are fixed and only F_a is changed to generate different wettability. Figure 4a shows a gently deposited drop on flat surfaces with different F_a, a function between F_a and the static contact angle (or the so-called Young angle) can be obtained. In this paper only the case that the fluid is hydrophobic on the flat solid surface is considered, so F_a is fixed at 70 and the related contact angle is around 118 °.

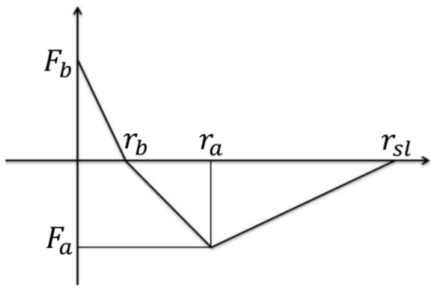

Figure 3 Solid/fluid interaction function curve

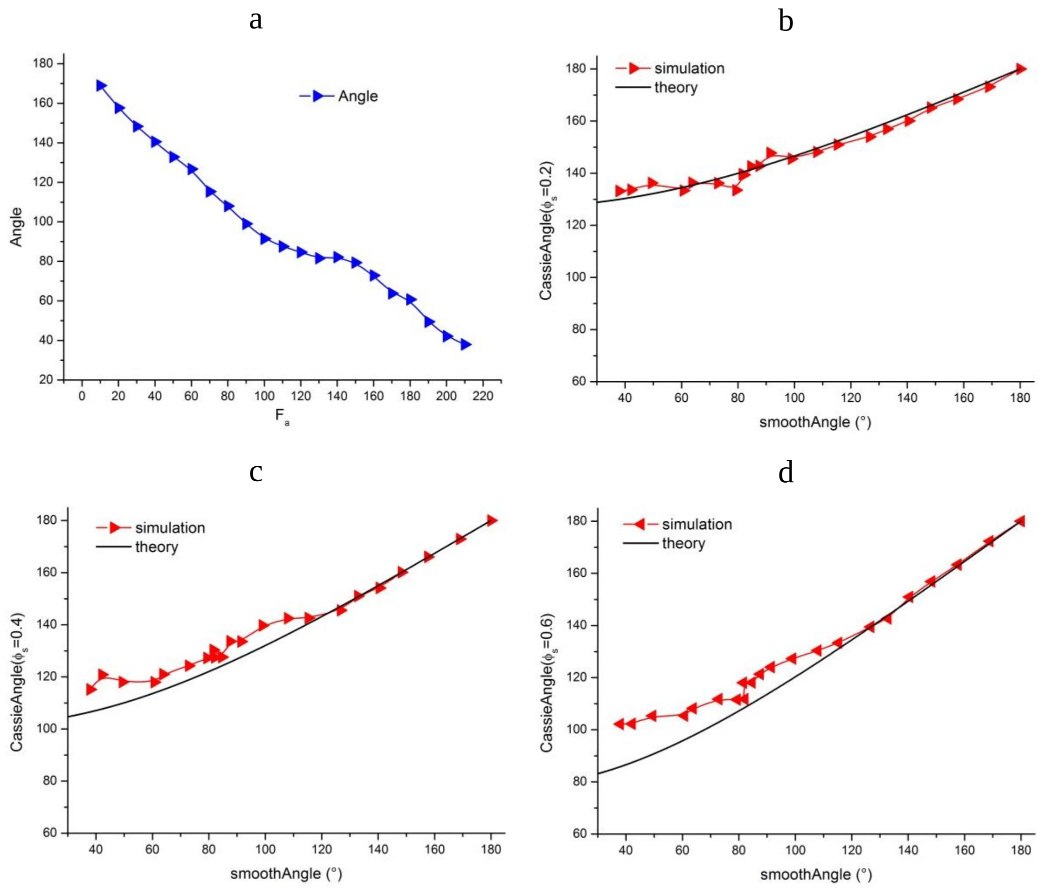

Figure 4 The contrast of simulated contact angles and Cassie theoretical values

Avoiding penetrating is another important problem and also for getting the ideal Cassie state the bounce-back reflections boundary condition is employed at the top of the pillars and air cushions which separate the drop from the solid substrate. Here the particles which penetrate the wall are forced back to the position of the last time step without changing their velocities. By these settings, any desired wettability can be obtained and also the algorithm is very robust. Furthermore the MDPD contact angle and the theoretically predicted angle (see the Cassie theory formula) are compared and a good agreement of them are shown in Figure 4b, 4c and 4d which correspond to $\emptyset_S = 0.2$, $\emptyset_S = 0.4$ and $\emptyset_S = 0.6$.

Measurement of the contact angle

Different from the fitting circle method [Koishi et al. (2009)], a simple but efficient numerical method by using geometrical computation is engaged to measure the contact angle between the solid surface and drop. Gently deposited drop is used to get the static contact angle. When the drop is stable on the solid surface, the position of the particles which enter the thin layer near the solid surface (upon the top of the pillars) are recorded, then, the difference between the maximum and the minimal values in the X direction is calculated as the length L of the contact line. Then, for all fluid particles, the maximum value in the Y direction is considered as the height H of the contact height. At last, a concise geometrical formula as follow is used to obtain the contact angle θ.

$$\theta = 2\tan^{-1}(2H/L) \tag{6}$$

Results and discussion

Time-Resolved Impact

Figure 5 shows snapshots of drops impacting on textured surfaces with $\emptyset_S = 0.2, 0.6$ and smooth surface ($\emptyset_S = 1$) at different velocities 0.1 and 10. The images in the first row show drops just before first contacting the surfaces. Before impacting, the drops are almost spherical with diameter D_0. After impacting, the drops spread until they reach a maximal spreading diameter, D_{max} (second row). The third row shows the minimal spreading diameter after the maximum spreading and in the last row most drops are in a stable state excepting the drop in second column which bounces back into the air. At high velocity (V=10), the drops are strongly deformed into a flat film much thinner than drop diameter D_0 in the middle region and gibbous rim emerging at the edge makes the drops look like a pancake, the similar result was observed by some other simulation [Eggers et al. (2010)] and physical experiments [Deng et al. (2013); Kim et al. (2012)]. In the retraction phase (third row and fourth row), the drop shape and state (rebound or pinning) depend on both the roughness of the surfaces and the deposited velocities. When deposited at high velocity, the drops elongate on the textured surfaces, but rebounding from the surface only happens at low $\emptyset_S$ ($\emptyset_S = 0.2$) and on the smooth surface the drop almost keeps its shape throughout the process. On the contrast, when the drops are deposited gently, the contact lengths are almost unchanged after the maximum spreading. We suppose that the kinetic energy of the drop is insufficient for the drop to move far and take shape of a pancake.

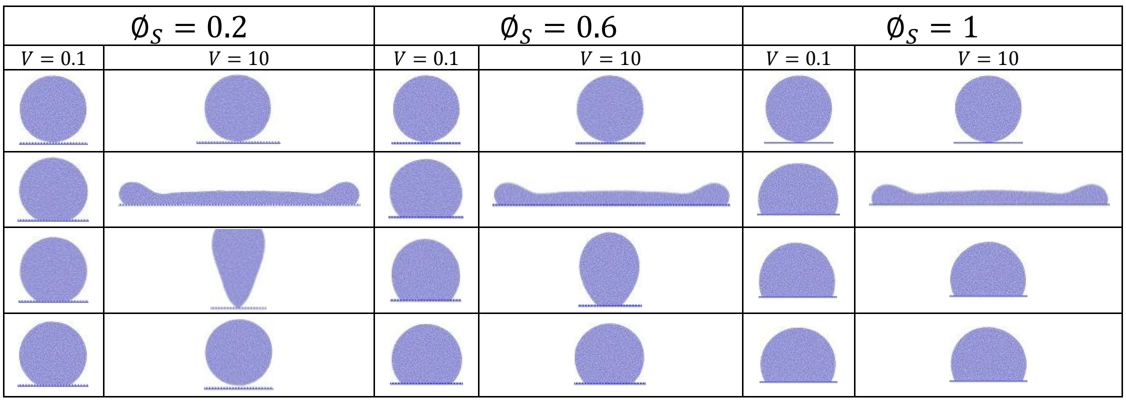

Figure 5 Time-resolved drop dynamics at different impact velocities

Time-Based Spreading Dynamics

The spreading diameter of the drop on the solid surfaces reflects the spreading and retraction dynamics and the energy dissipation of the impacting drop. For all surfaces, spreading diameters increase at first, then reach a maximum, and at last decreases. The maximal spreading diameter of the drop increases with increasing deposited V and spreading is always faster than retraction. Figure 6 shows that the temporal evolution of the spreading diameter depends on impact velocity significantly. Our simulation shows a good agreement with Deng's experiment [Deng et al. (2013)] in this period. Figure 7 shows two special snapshots in the drop spreading just before and after the drop reaching its maximum spreading diameter at V=10 and $\emptyset_S = 0.2$, the related dynamical contact angles of them can be seen as the advancing contact angle θ_A and receding contact angle θ_R [Deng et al. (2013)], the small difference between them indicates a small contact angle hysteresis. According to Deng' treatment, we also separate the retraction phase into two periods which can be divided at the time of their minimal spreading diameters respectively. In the first retraction period, the spreading diameters decrease with time monotonously, but there are some different phenomena between different textured surfaces: for low $\emptyset_S$ ($\emptyset_S = 0.2$), the drops start to rebound from low impact velocity (V=3) and from relative high velocity (V=6) for $\emptyset_S = 0.4$, but no rebounding occurs at $\emptyset_S = 0.6$ and smooth surface. In the second retraction period, the pinning drops undergo a slight fluctuation around their final spreading diameters respectively, that is because when the drops meet their minimal spreading diameter, the drops elongate (Figure 5, third row) and transform the retraction kinetic energy into interface energy and makes the drop unstable, after that, energy is dissipated through contact line fluctuating. From a DPD viewpoint, the dissipative force between solid particles and fluid particles can play an important role in this period. As a contrast, drop on the smooth surface ($\emptyset_S = 1$) only experiences the first retraction period, reflecting strong adhesion of the drop on the smooth surface. For the rebounding drops, the contact time (from the first contact with solid surfaces to the rebounding time) also depends on roughness and impact velocities: the higher the speed, the longer the contact time for the same textured surface and the contact time always shorter for the low $\emptyset_S$ under the same impact velocity(Figure 8). From all the four cases we also found that the equilibrated spreading diameters are independent of the impact velocities and larger at the high $\emptyset_S$, including $\emptyset_S = 1$, but not too obviously.

a b

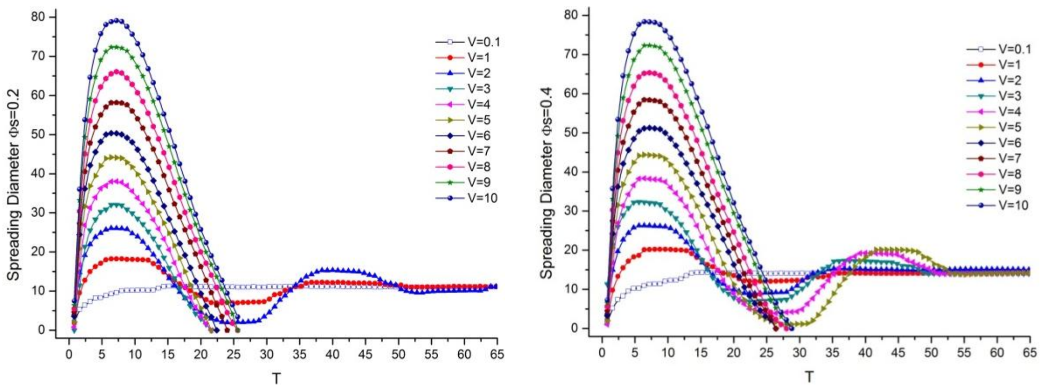

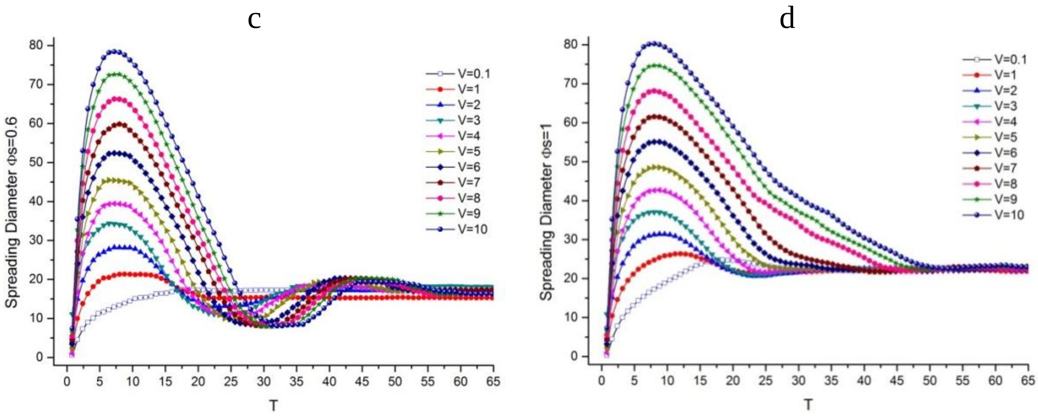

Figure 6 Time-based evolution of the spreading diameter

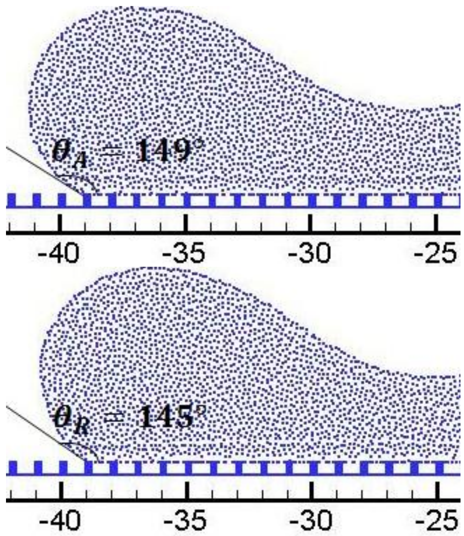

Figure 7 The advancing and receding "pancake"

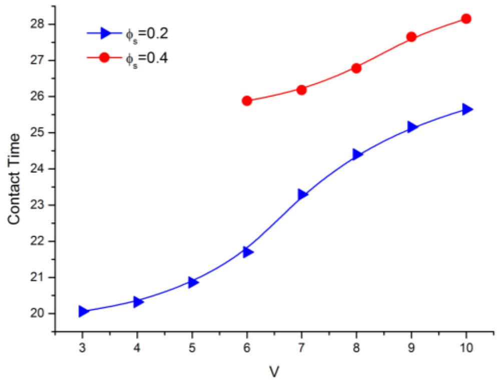

Figure 8 Contact time

Recently, a new viewpoint has been proposed trying to explain the contact line pinning by the so-called effective liquid Hammer pressure [Deng et al. (2009)]. Hammer pressure is caused by the hitting of the drop on the surface and the liquid is compressed which creates a shock wave that adds a vertical component to the velocity of the fluid, then, the shock wave relaxes as soon as it overtakes the moving contact line. In the future we will do more research about Hammer pressure. Figure 9 shows the compression of liquid.

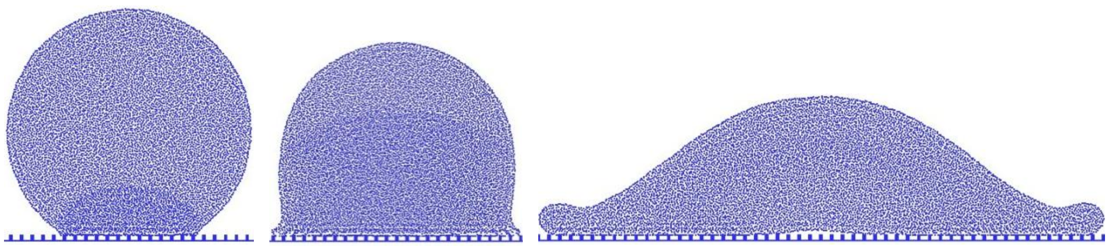

Figure 9 Drop at different moment just after impact ($\emptyset_S = 0.2$, V=10)

Conclusions

In this paper, a particle-based numerical method, MDPD, was built to simulate drop impact on textured surfaces. The simulated values show a good agreement with Cassie-Baxter theory. Also, the linear-jointed solid/fluid interaction and the contact angle measurement work well in the simulation.

After impacting on hydrophobic surfaces, drops undergo rebounding or pinning. The maximum spreading diameters and contact time depend on the different textured surfaces and velocities. At low velocities, the drops always pin on the surfaces and the maximum spreading diameters are small. When speeding the drops, at low $\emptyset_S$ the drop will rebound easily but pin at high $\emptyset_S$. The retraction phase shows two well-separated periods, i.e. a monotonous decreasing one and a fluctuant one. In the first period, energy stored in the deformation of the surface is transformed back into kinetic energy and this phase is inertia-dominated. The existence of a fluctuant period shows that the transforming between kinetic energy and the interface energy propel the movement of the contact line, which leads a dissipation of the total energy and make the drop stable at the end. At last, some evidences about Hammer pressure have been found and this may open a door for the farther research about the mechanism of drop spreading dynamics.

Acknowledgement

This work was supported by the National Natural Science Foundation of China (Grant No. 51276130, 10872152), the Specialized Research Fund for the Doctoral Program of Higher Education of China (Grant No. 20120072110037), and the Fundamental Scientific Research Foundation for the Central Universities of China (Grant No. 125065). The grants are gratefully acknowledged.

References

Barthlott, W. and Neinhuis, C. (1997) Purity of the sacred lotus, or escape from contamination in biological surfaces *Planta* 202, 1

Gao, X.F., Yan, X., Yao, X., Xu, L., Zhang, K., Zhang, J.H. and Yang, B. (2007) The dry-style antifogging properties of mosquitocompound eyes and artificial analogues prepared by soft lithography*Adv. Mater.* 19, 2213

Gao, X. and Jiang, L.(2004) Biophysics: water-repellent legs of water striders*Nature*432(7013),36

Wenzel,R.N.(1936) Resistance of solid surfaces to wetting by water,*Industrial & Engineering Chemistry* 28(8), 988

Cassie,A.B.D. and Baxter,S.(1944) Wettability of porous surfaces,*Transactions of the Faraday Society* 40,546

Singh, E., Thomas, A. V., Mukherjee, R., Mi, X., Houshmand, F., Peles, Y., Shi, Y.F. and Koratkar, N. (2013) Graphene Drape Minimizes the Pinning and Hysteresis of Water Drops on Nanotextured Rough Surfaces. *ACS nano*7(4), 3512

Kim,H., Lee,C., Kim,M.H.and Kim,J.(2012) Drop Impact Characteristics and Structure Effects of Hydrophobic Surfaces with Micro- and/or Nanoscaled Structures,*Langmuir* 28, 11250

Deng,X., Schellenberger,F., Papadopoulos,P., Vollmer,D. and Butt,H.J. (2013) Liquid Drops Impacting Superamphiphobic Coatings,*Langmuir* 29, 7847

Eggers,J., Fontelos,M.A., Josserand,C., and Zaleski,S. (2010) Drop dynamics after impact on a solid wall: Theory and simulations,*Physics of Fluids* 22, 062101

Warren, P.B.(2003) Vapour-liquid coexistence in many-body dissipative particle dynamics,*Phys. Rev. E* 68 066702

Trofimov, S.Y., Nies, E.L.F. and Michels, M.A.J. (2005) Constant-pressure simulations with dissipative particle dynamics,*The Journal of chemical physics* 123 144102

Hoogerbrugge,P.J. and Koelman, J.M.V.A. (1992) Simulating Microscopic Hydrodynamic Phenomena with Dissipative Particle Dynamics,*Europhys. Lett.* 19 155

Groot,R.D. and Warren, P.B. (1997) Dissipative particle dynamics: Bridging the gap between atomistic and mesoscopic simulation,*The Journal of chemical physics* 107 4423

Koishi, T., Yasuoka, K., Fujikawa, S., Ebisuzaki, T. and Zeng, X. C. (2009) Coexistence and transition between Cassie and Wenzel state on pillared hydrophobic surface,*Proceedings of the National Academy of Sciences* 106 8435

Deng, T., Varanasi, K.K., Hsu, M., Bhate, N., Keimel, C., Stein, J. and Blohm, M. (2009) Nonwetting of impinging droplets on textured surfaces, *Applied Physics Letters* 94, 133109